18TH WORLD CONFERENCE ON EARTHQUAKE ENGINEERING
WCEE2024
MILAN

MILAN, ITALY
30TH JUNE - 5TH JULY 2024

www.wcee2024.it

MULTIOBJECTIVE OPTIMIZATION OF A COUPLED WALL SYSTEM FOR TALL TIMBER BUILDINGS

Y. Miyazu[1] & C. Loss[2]

[1] Tokyo University of Science, Noda, Japan, miyazu@rs.tus.ac.jp

[2] The University of British Columbia, Vancouver, Canada, cristiano.loss@ubc.ca

Abstract: *Tall timber buildings that use mass timber products are attracting interest worldwide, and some project proposals are lined up even in countries with well-known high seismic hazards. A coupled wall (CW) system composed of cross-laminated timber (CLT) panels and energy dissipation devices (EDDs) is one of the most practical and effective methods to enhance the seismic performance of tall timber buildings. In the structural design of the CW system, the actual capacity of the EDDs becomes the design force to be used in detailing connections between the EDDs and the CLT panel, thus affecting the total cost of a project. In this research, the optimization method to minimize the capacity of steel link beams (SLBs) used as EDDs and the stress of the CLT panels was proposed and applied to an 18-story timber building. The optimization problem was formulated as a combinatorial multiobjective programming (MOP) problem composed of a two-stage approach and was solved by simulated annealing. The section forces of the CLT panel and the total yielding force of the SLBs were defined as the objective functions and the maximum inter-story drift was assigned as the constraint function of the problem. The value of the objective and the constraint functions were evaluated by time history response analyses using 10 ground motion records selected from the PEER NGA-West2 Database. The proposed method was effective in finding the minimal capacity of SLBs and providing structural designers with a computational strategy to design CW systems in tall timber building applications.*

1. Introduction

1.1. Tall mass timber buildings

Cross-laminated timber (CLT), glued laminated timber (GLT), laminated veneer lumber (LVL), and other mass timber products accepted in most of the building codes are designers' first choice for tall applications upon members and structural assembly are well-engineered to attain limit-state design requirements (Safarik 2022). Currently, CLT is the most used mass timber product for structural walls, floors, and diaphragms in multi-story timber buildings. With bearing walls of CLT multi-panel segments, the two standard construction systems are platform-type and balloon-type (Karacabeyli and Lum 2022). The design of platform-type structures is usually limited to low- and mid-rise buildings since the floor panels have to carry the load in a perpendicular-to-grain direction, while balloon-type structures with cantilevered walls are preferred for tall buildings. With the current construction market moving towards high-rise buildings, the lagging of design provisions, for instance, in the 2020 National Building Code of Canada (NBC) (NRC 2020) and 2019 Canadian Standard Engineering Design in Wood (CSA 2019), pushes for research and codification of balloon-type systems (Chen and Popovski 2024, Yang et al. 2022). In addition, some limitations also arise when designing buildings in earthquake-prone countries, such as Canada, the United States, and Japan.

For earthquake-resistant tall timber buildings, hybrid timber-concrete or timber-steel structural systems built by pairing a timber-based gravity load-resisting system (GLRS) with a concrete or steel lateral load-resisting system (LLRS) have been actively developed and widely used in recent construction. For example, the 18-story 'Brock Commons' building (naturally: wood 2016) in Vancouver, Canada, and the 25-story 'Ascent' (Fernandez et al. 2020) building in Milwaukee, USA, have two concrete cores performing as vertical elements of its LLRS. The 12-story residential building 'Tallwood 1' (Aspect Structural Engineers 2023) in Langford, Canada, uses eccentrically-braced steel frames as the LLRS, rising from the 2nd story to the top. The main advantage of using concrete or steel LLRS vertical elements for tall timber buildings is given by consolidated engineering practice and knowledge in system detailing, which yields reduced construction costs.

Although tall buildings using mass timber elements in the GLRS and LLRS have already been constructed in some areas, they are limited to applications where lateral seismic forces are low or negligible. For example, Norway's Treet and Mjøstårnet buildings were designed by adopting timber bracing systems as LLRS to withstand mainly wind loads.

1.2. Coupled wall system for timber buildings

Coupled wall (CW) systems composed of CLT or LVL wall panels and energy dissipation devices (EDDs) have been studied recently to provide tall buildings with timber-based LLRSs (OSU/PSU 2017, NHERI Tall Wood 2023). Steel link beams (SLBs) and U-shaped flexural plates are generally used as EDDs for the CW system, and experimental and numerical studies on the CW system for timber buildings have been conducted by (Iqbal et al. 2015, Ganey et al. 2017, Moerman et al. 2022, Dires and Tannert 2022, Teweldebrhan and Tesfamariam 2022). These previous researches pointed out that the stiffness and strength of the connections between a coupled wall and an EDD play an essential role in enhancing the energy dissipation performance of EDDs. Compared to concrete-to-EDD connections or steel-to-EDD connections, timber-to-EDD connections tend to have lower stiffness and strength due to the flexibility of bolted or screwed connections.

One option to ensure the effectiveness of EDDs is to improve the mechanical performance of the timber-to-EDD connection. Shulman and Loss (2023a, 2023b) developed a high-performance grout-reinforced shear connector that possesses high stiffness and strength, and Feujofack and Loss (2023) developed a 3D finite-element model to simulate its non-linear behavior under static loading conditions. The other option is to reduce the force acting at the connection as much as possible by minimizing the capacity of EDDs while satisfying the required seismic performance of the building. The latter approach is versatile and could be applied to any CW system; however, the specific methodology is not provided, so it is out of reach for most structural designers.

1.3. Structural optimization for timber buildings

Design optimization is a powerful tool for sizing structural assemblies and members under constraints given by design criteria. Various optimization methods have been proposed and applied to several building structural types, such as trusses, spatial trusses, or frames (Ohsaki 2010). Work has also been published for optimization approaches applied to timber structures. Poh'sie et al. (2016) used a genetic algorithm to optimize the parameters of a tuned mass damper for a seven-story CLT building. Mam et al. (2020) focused on finding the optimal shape for timber-braced frames and investigated the influence of a semi-rigid connection on the optimization results. Das and Tesfamariam (2022) proposed a shape memory alloy-based outrigger system for tall timber buildings and optimized its property by solving multiobjective programming problems using some meta-heuristic optimization algorithms. This research shows the possibility of utilizing optimization techniques for timber buildings to upgrade their lateral or seismic performance; however, applying the optimization approach to the CW system for tall timber buildings is not well-studied.

2. Method

2.1. Building overview

The footprint, height, and design specs of an 18-story timber-concrete hybrid building located in Vancouver, Canada (naturally: wood 2016) are used to develop the case study building of this work. With reference to Figure 1a, the two reinforced concrete (RC) cores forming the building's LLRS are replaced by CWs. These latter are assembled with CLT walls, SLBs mounted side-ends between CLT walls, and self-centering devices (SCDs) installed at the base of each CLT wall, as shown in Figure 1b. The lower end of the CLT wall is connected to a steel coupler pin connected to the RC foundation. In addition, the RC podium of the original building is removed in the reference building. As a result, the superstructure gravity system comprises GLT

and parallel strand lumber (PSL) columns and CLT floor panels. GLT and PSL members and CLT panels have paired properties and sections as per the original UBC Brock Commons building.

In both main directions, four CWs with SLBs are installed symmetrically to the center of the building, as illustrated in Figure 1a. The width and thickness of the 9-ply E1M5 stress-grade CLT walls are 3 m and 315 mm, respectively. The cross-section of the SLB is selected from the list of readily available W-shaped steel sections database (CISC 2016), and the optimal cross-section is found through an optimization process explained in Section 2.4. Regarding the self-centering system at the base of the building, the installed disc-spring-type devices perform in non-linear elastic behavior, dissipating energy through friction between the contact surfaces (Fang et al. 2021). The design of the joints of the balloon-type CLT segments is assumed to deploy a monolithic continuous wall, with negligible deformation of the connectors compared to the inherent lateral deflection of the CLT panels. Similarly, the CLT-to-SLB connections and the CLT-to-steel coupler connections are also assumed to be capacity-protected and perform with rigid behavior.

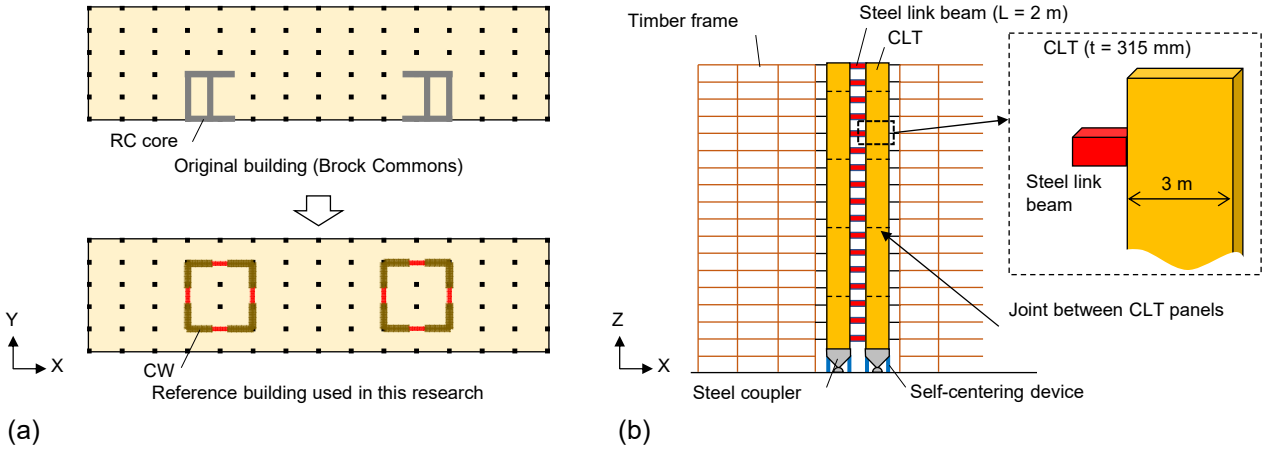

Figure 1. Conceptual drawing of an 18-story timber building with CWs: (a) Plan view, (b) Elevation view.

2.2. Numerical modelling

System-level mechanical properties and behavior of the CLT panels of the CW system were modeled through Euler–Bernoulli beam-type elements. Homogeneous fictitious properties of wood were tailored to a CW system with CLT panels modeled through layered shell elements (Figure 2a) under uniformly distributed lateral loads, as illustrated in Figure 2b. Four-node thick-shell elements based on Reissner-Mindlin's plate theory were used for the shell-type elements, and the mechanical elastic properties of wood were assigned per the Canadian CLT Handbook (FPInnovations 2019), as detailed in Table 1. The layered shell modeling and its static loading analysis were executed in the SAP2000 (CSI 2023) framework.

In Figure 3, the two-dimensional finite-element (2DFE) model of the reference building was developed in OpenSees (McKenna 2010). The equivalent single CW-type model comprised two CLT wall panels, four SCDs, and 17 SLBs. CLT wall panels were modeled via an *elasticBeamColumn* element with an assigned fictitious Young's modulus of 6849 N/mm^2. SLBs were connected using 1.5 m long rigid beams. SLBs were modeled as a combination of *elasticBeamColumn* elements and rotational *zeroLengh* elements at their ends with bi-linear hysteresis behavior. Connected to the CLT wall panel via rigid beams, a *twoNodeLink* element with non-linear elastic spring was used for each SCD. The yielding moment (f_y) of the *zerolengh* element for the SLB was calculated using its plastic modulus, and the initial stiffness (K_1) and hardening ratio (K_2/K_1) were adjusted following the method proposed by Ibarra and Krawinkler (2005). Two yield force levels, f_y = 1000 kN and 2000 kN, were assigned to the *twoNodeLink* element simulating the SCD, with a yield deformation (d_1) set at 5 mm. The post-yield stiffness (K_2) was set at 10% of the initial stiffness (K_1). The damping matrix was constructed by assuming stiffness-proportional damping and the damping ratio of 3% was assigned to the 1st mode of the model.

To account for the P-Delta effects, a leaning column was included in the model and attached to the two CLT wall panels through rigid *truss* elements. Mass of each node in the leaning column was assigned based on the gravity load at each story, evaluated via elastic static analysis of the three-dimensional finite-element (3DFE)

model shown in Figure 4. The elastic static analysis of the 3DFE model was performed with the 1D+0.5L+0.25S load combination in accordance with the NBC (NRC 2020); where D, L, and S represent dead, live, and snow loads, respectively. The dead load and live load, listed in Table 2, were assessed to comply with the design documentation of UBC Brock Commons.

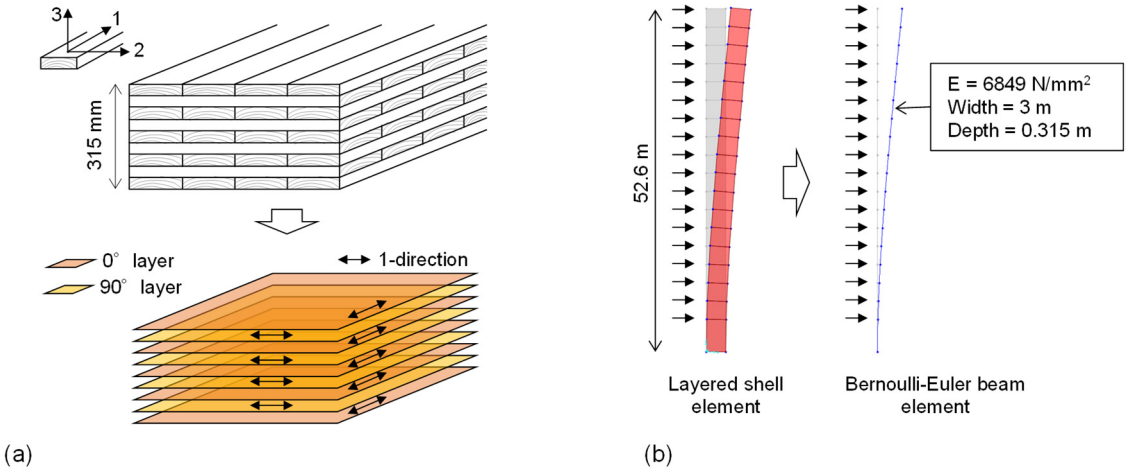

Figure 2. Modelling of the CLT wall panel: (a) Layered shell element for the CLT, (b) Equivalent Bernoulli-Euler beam for the CLT wall panel.

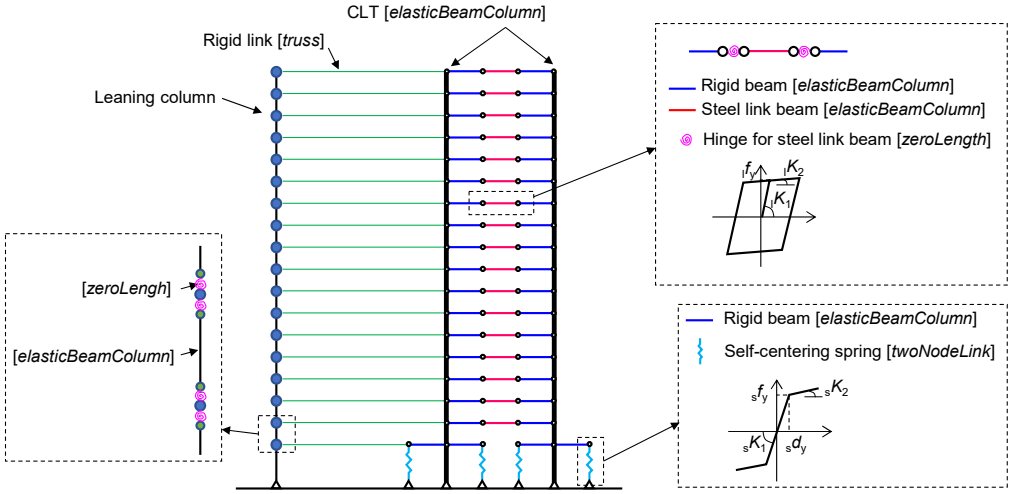

Figure 3. Two-dimensional finite-element model developed in OpenSees for the reference building.

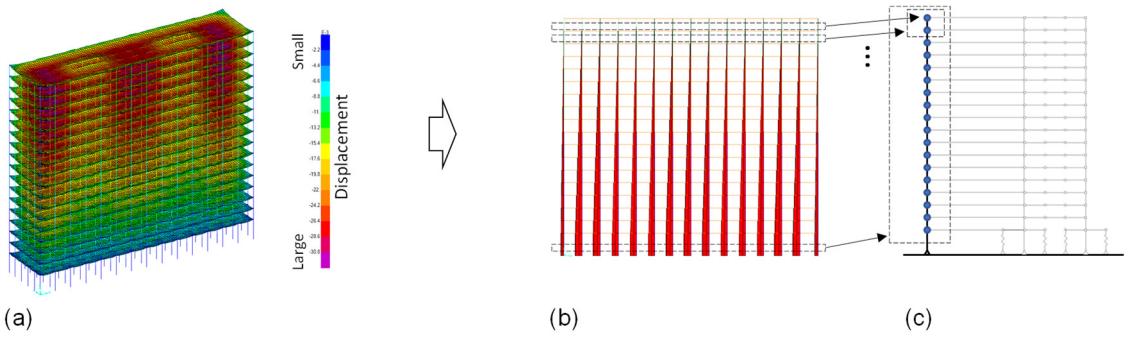

Figure 4. Calculation of mass assigned to the leaning column; (a) Static analysis on the 3DFE model, (b) Axial force of the columns, (c) The leaning column in the 2DFE model.

Table 1. Mechanical properties of shell-type element for the CLT.

Property (Unit)	0°–layer	90°–layer
E_1 (MPa)	12,400	9,500
E_2, E_3 (MPa)	413	317
G_{12}, G_{13} (MPa)	755	594
G_{23} (MPa)	78	59

Table 2. Dead loads and live loads applied to the floors and the roof in the static analysis on 3DFE model.

Component	Dead load (kPa)	Live load (kPa)
Floor (room)	2.25	1.9
Floor (corridor)	1.25	4.8
Roof	1	0

2.3. Ground motion selection

Five ground motions were selected based on Baker's conditional mean spectrum (CMS) (2011). Specifically, Baker and Lee's algorithm (2018) was used to select the ground motions from the PEER NGA-West2 Database. A 2% probability of exceedance in 50 years, mean distance and magnitude at $S_a(2.0)$ for Vancouver, Canada, were used in the NBCC 2015 seismic hazard disaggregation method by Halchuk et al. (2019) and the ground motion selection. Figure 5a shows the acceleration response spectrum of each selected ground motion, whereas Figure 5b provides their acceleration time records. The bi-directional characteristics of the ground motion were accounted for in the time history response analysis.

The CMS has $S_a(2.0)$ of 0.26 g and shows a flat shape in the range from 0.2 s to 2.0 s, while it decreases in the period range larger than 2.0 s. The response spectra of selected ground motions are almost within the lines of mean ± two standard deviations. As for acceleration time records, maximum acceleration and duration vary among ground motions. RSN1528 has the largest maximum acceleration, 0.317 (g), which is 5.7 times larger than RSN2459.

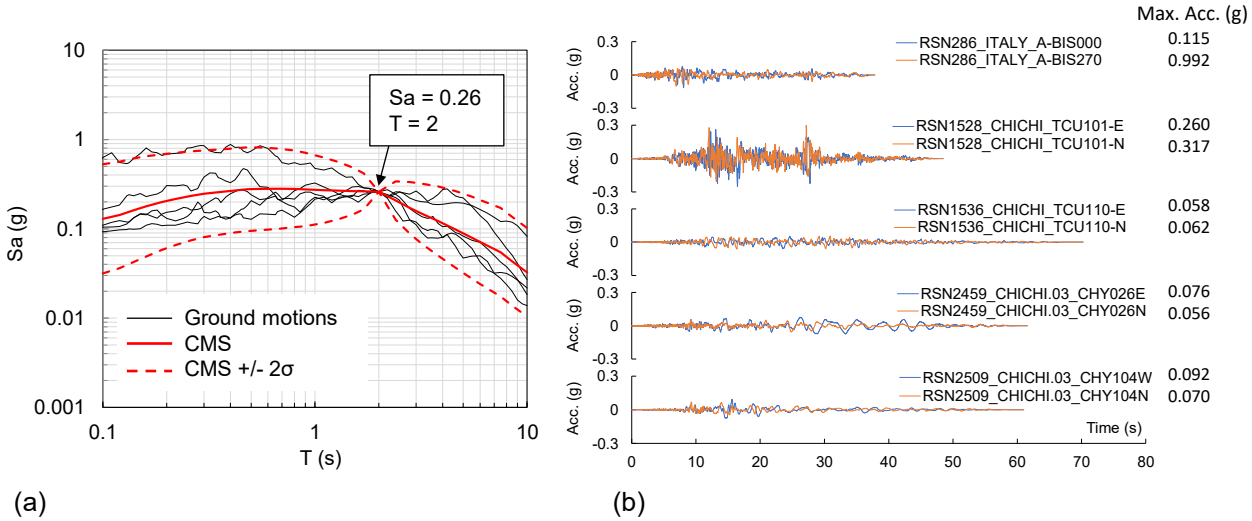

Figure 5. Selected ground motions: (a) Acceleration response spectrum (h = 0.05), (b) Acceleration time records (bi-directional records for one ground motion).

2.4. Optimization method

This study focused on the cross-section size optimization of the SLBs. From the (CISC 2016) database, ten W-shaped standard steel sections were considered candidates for sizing the SLBs, as detailed in Figure 6. Each W-shaped section was assigned the integer variable $x \in \{1,2,\ldots,11\}$; 1 is intended for the smallest cross-section, whereas 11 is for the largest, as shown in Figure 6a. The yield bending moment resistance and yield

shear resistance of the SLBs are proportional to the variable *x*, as shown in Figures 6b and c, respectively. Since *x*-steps are approximately linear to the yield moment and yield shear forces, the forces acting on the connections between the SLB and the CLT wall panel and the stress in the CLT wall panel are expected to be reduced by decreasing *x* through the optimization process.

Name	Depth (mm)	Width (mm)	Design variable *x*
None	-	-	1
W200x31	210	134	2
W360x39	353	128	3
W250x73	253	254	4
W410x67	410	179	5
W460x74	457	190	6
W460x89	463	192	7
W530x92	533	209	8
W530x101	537	210	9
W610x101	603	228	10
W610x113	608	228	11

(a)

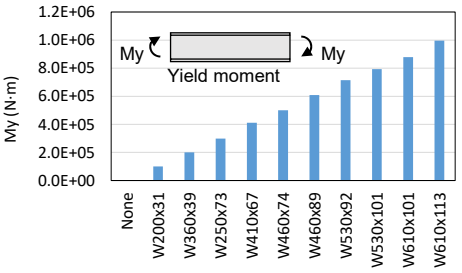

(b)

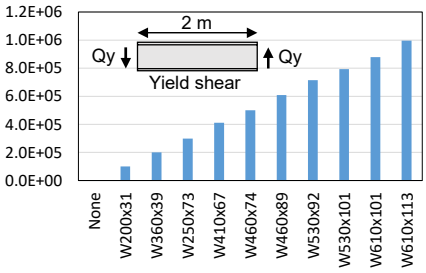

(c)

Figure 6. Candidates for the cross-section size of the SLBs; (a) Depth, width, and x of the selected W-shape steel sections, (b) Yield moment resistance, (c) Yield shear resistance.

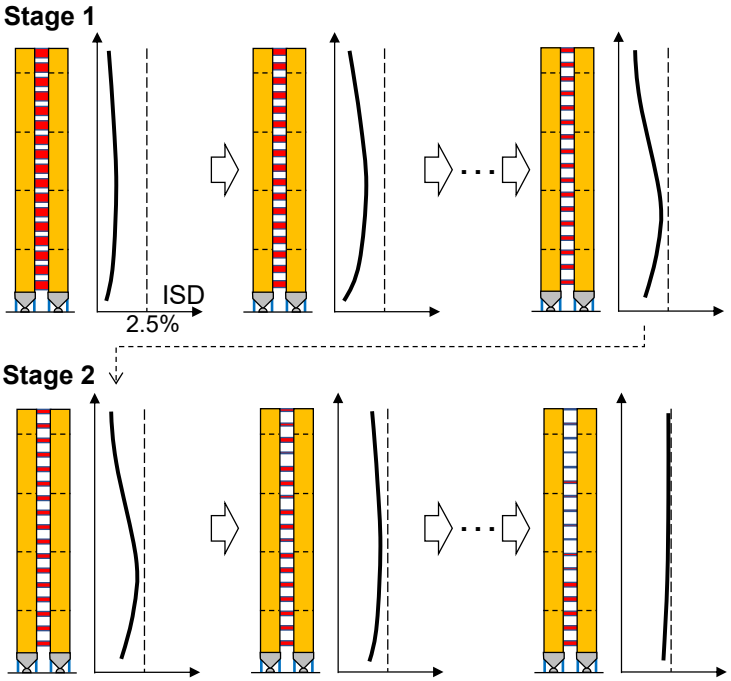

(a)

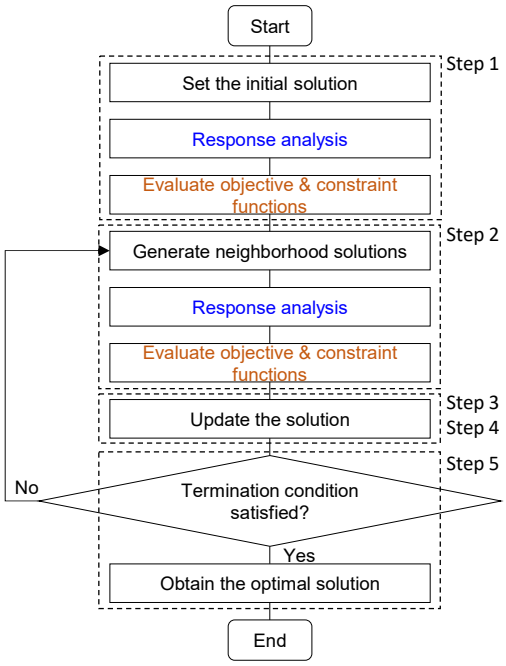

(b)

Figure 7. Concept of the two-stage approach for the optimization; (a) Schematical explanation of Stages 1 and 2, (b) Flow chart of Stage 2.

The optimization consists of two stages as schematically explained in Figure 7. In Stage 1, the design variable *x* was uniformly decreased from 11 to 1 and the maximum inter-story drift (ISD) of each model was evaluated by time history response analysis. Here, define $d_{\mathrm{MSD}}(\mathbf{x})$ as

$$d_{\mathrm{MSD}}(\mathbf{x}) = \bar{d}_{\max}(\mathbf{x}) + \sqrt{\frac{1}{10}\sum_{i=1}^{10}\left({}_i d_{max}(\mathbf{x}) - \bar{d}_{\max}(\mathbf{x})\right)^2}, \quad \bar{d}_{\max}(\mathbf{x}) = \frac{1}{10}\sum_{i=1}^{10} {}_i d_{max}(\mathbf{x}) \tag{1}$$

where ${}_i d_{max}(\mathbf{x})$ is the maximum ISD for the i^{th} ground motion input and $\mathbf{x}$ is the vector of design variables x. Then, the solution which has $d_{\text{MSD}}(\mathbf{x})$ less than 2.5% with minimum x was selected as the best solution in Stage 1. In Stage 2, x was further decreased by solving the optimization problem formulated as follows:

$$\text{Minimize} \quad F_1 = Q_{\text{MSD}}(\mathbf{x}), \quad F_2 = M_{\text{MSD}}(\mathbf{x}), \quad F_3 = N_{\text{MSD}}(\mathbf{x}), \quad F_4 = \sum_{i=1}^{17} x_i \tag{2a}$$

$$\text{subject to} \quad d_{\text{MSD}}(\mathbf{x}) \le 2.5\% \tag{2b}$$

$$1 \le x_i \le x_i^U, \quad (i = 1, \ldots, 17) \tag{2c}$$

where $Q_{\text{MSD}}(\mathbf{x})$, $M_{\text{MSD}}(\mathbf{x})$, and $N_{\text{MSD}}(\mathbf{x})$ are calculated by Equation 1 by replacing ${}_i d_{max}(\mathbf{x})$ to shear force ${}_i Q_{max}(\mathbf{x})$, moment ${}_i M_{max}(\mathbf{x})$, and axial force ${}_i N_{max}(\mathbf{x})$, respectively. In the constraint functions defined in Equation 2c, x_i^U is the upper bound for x_i and is set at the same value of x as the best solution obtained in Stage 1.

This optimization problem is classified as a combinatorial multiobjective programming (MOP) problem. Since the computational time required to evaluate the objective and constraint functions is long due to performing non-linear time history analysis, simulated annealing (SA), which uses the following algorithm based on the method proposed by Jilla and Miller (2001), was adopted to solve this optimization problem.

Step 1: The best solution obtained in Stage 1 is set to the initial solution $\mathbf{x}^{(0)}$. Set the initial temperature and the iteration counter $T_0 = 1$ and $k = 0$, respectively.

Step 2: Randomly generate 15 neighborhood solutions $\mathbf{x}^*$ of $\mathbf{x}^{(k)}$, and evaluate their objective and constraint functions by time history analysis. Then, calculate ΔF defined by

$$\Delta F = \frac{1}{4}\left(\sum_{i=1}^{4} \frac{F_i(\mathbf{x}^*) - F_i\left(\mathbf{x}^{(k)}\right)}{\delta_i}\right) \tag{3}$$

where $F_i(\mathbf{x})$ is the *i*-th objective function and δ_i is the same values as $F_i\left(\mathbf{x}^{(0)}\right)$.

Step 3: If the minimum ΔF among the neighborhood solutions is smaller than zero, or if the random number $0 \le R < 1$ is smaller than P defined by Equation 4, accept its $\mathbf{x}^*$ as $\mathbf{x}^{(k+1)} = \mathbf{x}^*$; otherwise, let $\mathbf{x}^{(k+1)} = \mathbf{x}^{(k)}$.

$$P = \exp\left(-\frac{\Delta F}{s T_k}\right) \tag{4}$$

where s is the scaling parameter and is set at 0.448 to let $P = 0.8$ when $\Delta F = 0.1$ and $T_k = 1$.

Step 4: Update the temperature to $T_{k+1} = 0.9 T_k$.

Step 5: If k becomes 30, or if the constraint function defined by Equation 2b is not satisfied consecutive five times, terminate the process; otherwise, set k to $k + 1$ and go to Step 2.

Optimization was performed on two building models: Model 1000 and Model 2000. Model 1000 has the SCD with the yield force f_y = 1000 kN, whereas in Model 2000, f_y = 2000 kN. The other parameters remain the same in both models.

3. Results and discussion

3.1. Results

Figure 8 shows the maximum response in terms of ISD and acceleration based on the initial solution in Stage 1, as well as the maximum value of shear force, bending moment, and axial force of the CLT wall panel. Gray lines indicate the response for each ground motion, whereas red solid and dashed lines represent the mean values, as well as the mean values plus the standard deviation, respectively. Figure 9 summarizes the optimization results of Models 1000 and 2000. Specifically, the leftmost figure shows the design variable values for the initial solutions in Stage 1 and Stage 2, as well as the optimal solution. In the other figures, the mean plus standard deviation values of ISD, acceleration, CLT wall panel shear force, moment, and axial force are plotted against the story level. Blue and orange lines refer to the initial solution in Stages 1 and 2, respectively,

whereas the optimal solution is reported in gray. The maximum values among all the story or floor levels are listed in Table 3. Table 4 lists the natural 1st to 3rd mode periods extracted from the initial solutions in Stages 1 and 2, and the optimal solution.

3.2. Design implications for Model 1000

Seismic responses of the initial solution in Stage 1 show that the difference between Models 1000 and 2000 is minor except for the ISD and the bending moment in the CLT wall panel at the lower story level. The high capacity of the SCD works to constrain the lower end of the CLT wall panel, increasing the CLT wall panel moment and decreasing the ISD below the 5th story.

Results from the design variable index show that the cross-section of the SLBs was reduced to W-460×89 (i.e., x = 7), moving from Stage 1 to Stage 2. For 8 of the 17 SLBs installed in the middle- to lower stories, the cross-section was further reduced to W-460×74 in the final step of the optimization process. Through the optimization reaching the maximum ISD of 2.5%, a reduction of the shear and axial forces was shown at the base of the building. Acceleration at the middle- to upper floors was also reduced through the optimization.

Precisely, the CLT wall panel shear and axial forces were decreased by decreasing the cross-section of the SLBs from the base to the mid-height of the building. With reference to Table 3, the maximum shear and axial forces were reduced by 16% and 34% in Stage 1 and 4% and 5% in Stage 2 from the initial solution in Stage 1, respectively. The maximum acceleration was reduced by 12% from the initial solution in Stage 1, and finally the acceleration on the 1st floor (i.e., input acceleration) became the largest on all the floors. However, the maximum moment of the optimal solution increased by 17% from the initial solution in Stage 1 through the optimization process, and it was shown dominant around the 6th story. This indicates that the connection between CLT wall panels should be carefully designed to transfer the increased moment.

The 1st, 2nd, and 3rd modes' natural periods of the optimal solution increased by 9%, 13%, and 19%, respectively, from the initial solution in Stage 1, showing that the higher modes were more affected by the capacity of the SLBs. Compared with the original Brock Commons, the fundamental period of the optimal solution is 1.7 times longer.

3.3. Model 2000 versus 1000

The cross-sections of the SLB were reduced to W-460×74 (i.e., x = 6) in Stage 1, then those in the upper stories were further reduced to W-410×67 or W-250×73 in Stage 2. The ISD in the middle to upper stories increased by decreasing the cross-section of the SLBs, whereas the ISD was slightly reduced in the lower stories.

The distribution of the ISD along the height of the building shows a significant difference between Models 1000 and 2000. As seen in Figure 9, the IDA in the lower stories was almost unchanged after the optimization process, indicating that the capacity of the SCD governed the ISD in the lower stories, and the SLB had a negligible effect on it. Regarding the moment of the CLT wall panel of the optimal solution, the maximum value of Model 2000 is 1.5 times larger than that of Model 1000, which is mainly caused by the larger yielding force of the SCD.

Compared to the design variables of the optimal solutions, the SLB with a smaller cross-section was selected in Model 2000. This indicates that the high-capacity SCD can reduce the required force of the SLB, resulting in mitigation of the force acting on the CLT-to-SLB connection. However, since the moment generated in CLT wall panels increases in Model 2000, the CLT-to-CLT connection should be designed stiffer than that of Model 1000.

3.4. Outlook

The capacity of the SCD affects the optimal cross-section of the SLB, the distribution of ISD, and the maximum moment of the CLT wall panel. High-capacity SCDs lead to smaller SLB cross-sections, smaller ISD in the lower stories, and larger CLT wall panel bending moments in the lower levels in the optimal solutions. From the viewpoint of the design of CLT-to-SLB connections, the high-capacity SCD has an advantage since it can reduce the capacity of SLBs; on the other hand, the high-capacity SCD requires higher stiffness and strength on the joint between the CLT wall panels. This means that there could be an optimal capacity of the SCD, and the capacity of SCDs should be included in the design variable set of the optimization problem. Furthermore, the forces acting at CLT joints and CLT-to-SLB connections should be considered as objective or constraint functions, with modelling these connections in FE models. Based on the limited case studies in this research,

Model 1000 seems to be preferable since the ISD is uniform along the height of the building and the CLT wall panel moment is much smaller than Model 2000. However, as mentioned above, more elaborate studies, which involve relevant factors such as precise modelling of the connections, torsional response of the building, the effect of diaphragms, other earthquake levels, and the number of ground motions, are required to obtain a reliable and feasible optimal solution.

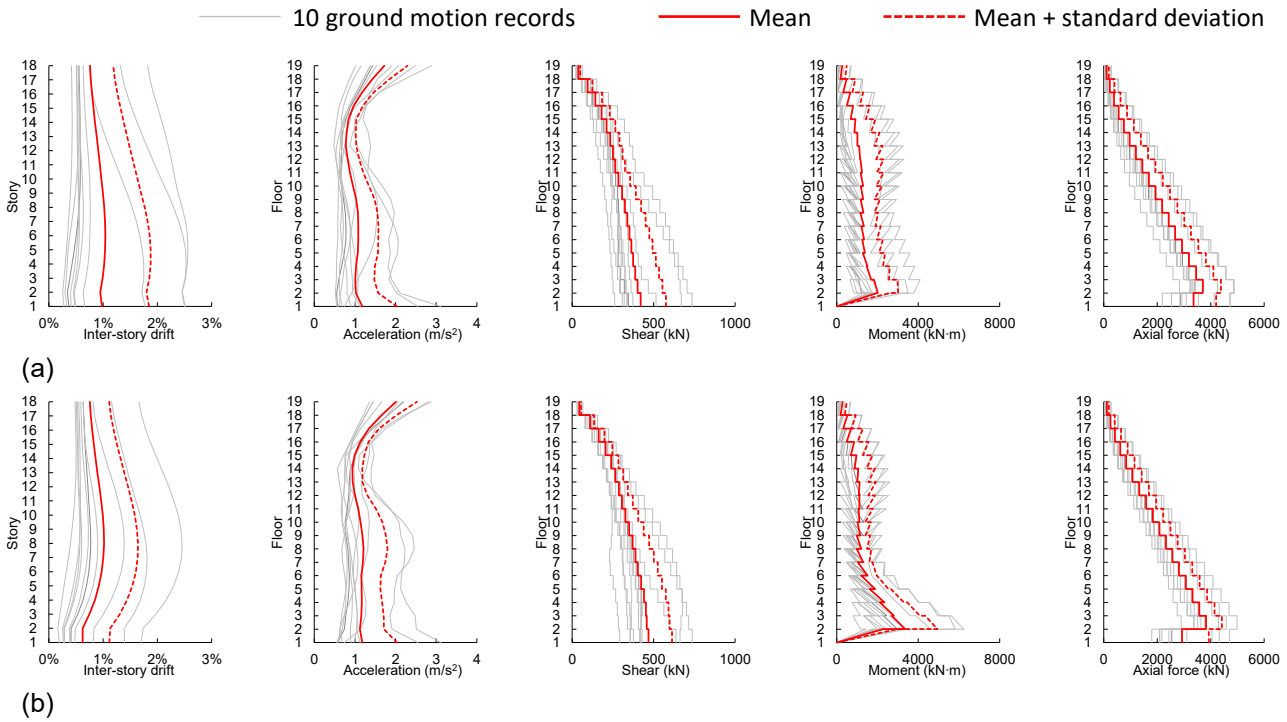

Figure 8. Maximum responses of initial solution in Stage 1; (a) Model 1000, (b) Model 2000.

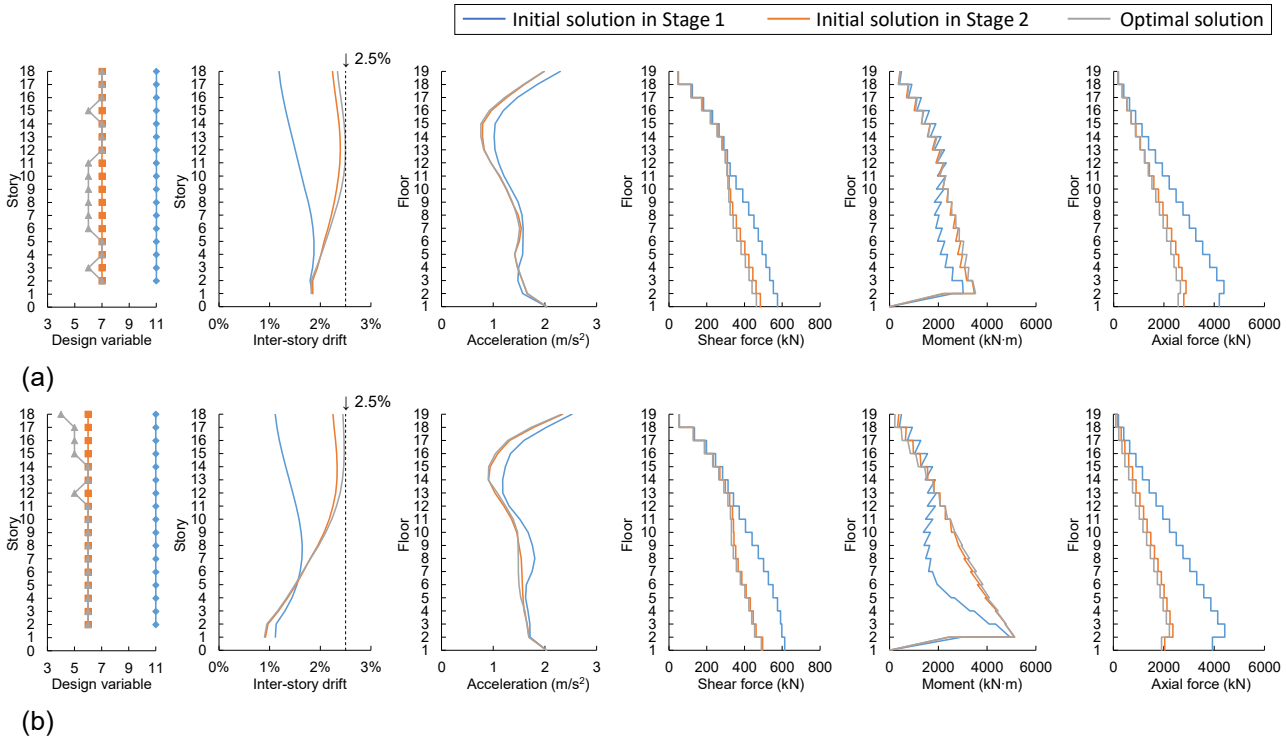

Figure 9. Design variable and seismic responses of each solution; (a) Model 1000, (b) Model 2000.

Table 3. Maximum values of the mean + standard deviation among all the story or floor levels.

Response (unit)	Model 1000			Model 2000		
	Initial solution in Stage 1	Initial solution in Stage 2	Optimal solution	Initial solution in Stage 1	Initial solution in Stage 2	Optimal solution
ISD (%)	1.88	2.40	2.50	1.64	2.33	2.49
Acceleration (m/s^2)	2.30	2.03 (0.88)	2.03 (0.88)	2.52	2.35 (0.93)	2.32 (0.92)
Shear force (kN)	575	484 (0.84)	463 (0.81)	613	496 (0.81)	489 (0.80)
Moment (kN·m)	3016	3475 (1.15)	3518 (1.17)	4943	5133 (1.04)	5108 (1.03)
Axial force (kN)	4382	2880 (0.66)	2654 (0.61)	4419	2361 (0.53)	2219 (0.50)

* The value in parentheses is a ratio to the response of the initial solution in Stage 1.

Table 4. Natural periods (s) up to 3rd mode of Models 1000 and 2000.

Mode	Model 1000			Model 2000		
	Initial solution in Stage 1	Initial solution in Stage 2	Optimal solution	Initial solution in Stage 1	Initial solution in Stage 2	Optimal solution
1st mode	3.08	3.32 (1.08)	3.37 (1.09)	2.91	3.20 (1.10)	3.21 (1.10)
2nd mode	0.77	0.86 (1.12)	0.87 (1.13)	0.72	0.83 (1.15)	0.84 (1.17)
3rd mode	0.32	0.37 (1.16)	0.38 (1.19)	0.31	0.37 (1.19)	0.38 (1.23)

* The value in parentheses is a ratio to the initial solution in Stage 1.

4. Conclusions

This research proposed a coupled wall system composed of CLT panels, steel link beams, and self-centering devices for an 18-story tall case study timber building with the footprint, building height, and gravity load resisting system per the existing UBC Brock Commons building in Vancouver, Canada. Towards the sizing of steel link beams of the coupled wall system, an optimization framework was formulated via a combinatorial multiobjective programming problem in order to minimize their cross-sections. A two-stage approach for the optimization problem was proposed and solved by using simulated annealing. The following conclusions can be drawn:

- The optimal cross-section of the steel link beam was affected by the capacity of the self-centering device. A high-capacity self-centering device leads to a smaller required cross-section for the steel link beam
- The shear and axial forces in the CLT wall panels decreased by reducing the cross-section size (i.e., the yielding moment and shear force) of the steel link beams, whereas the bending moment of the CLT increased, especially in the middle to lower stories. This indicates that the connection between the two CLT wall panels should be properly capacity-protected to resist section forces
- The fundamental periods of the optimal solutions were over 3 seconds, which is longer than the Brock Commons' fundamental period; this latter estimated as 2 s from the structural design report
- The capacity of the self-centering device also affected the distribution of ISD and the maximum moment of the CLT wall panel; thus, this parameter could be accounted for design variables in the optimization problem
- To obtain more reliable and feasible optimal solutions, it is desired to model joints and connections in the FE model, evaluate the torsional response of the building and the effect of diaphragms, consider other earthquake levels, and increase the number of ground motions in the modeling and optimization process.

5. Acknowledgements

This research was funded by the Government of British Columbia through the FII Wood First Program and by the Natural Sciences and Engineering Research Council (NSERC) of Canada through the Discover Program grant number RGPIN-2019-04530, and Discovery Launch Supplement, grant number DGECR-2019-00265.

The financial support provided by the Japan Society for the Promotion of Science (JSPS) through JSPS KAKENHI Grant Number JP22K04421 is also acknowledged.

6. References

Aspect Structural Engineers (2023). District 56 Tallwood 1. https://aspectengineers.com/portfolio/tallwood/. Accessed 27 October 2023.

Baker J.W. (2011). Conditional mean spectrum: tool for ground-motion selection, *Journal of Structural Engineering*, 137(3): 322–331.

Baker J.W., Lee C. (2018). An Improved Algorithm for Selecting Ground Motions to Match a Conditional Spectrum, *Journal of Earthquake Engineering*, 22(4): 708-723.

Canadian Institute of Steel Construction (CISC) (2016). *Handbook of Steel Construction - 11th Edition*, Ontario: Canadian Institute of Steel Construction.

Chen Z., Popovski M. (2024). Theoretical Building Height Limits of Balloon Mass Timber Shear Wall Systems, *Journal of Structural Engineering***,** 150(1): 04023194.

Computers and Structures, Inc. (CSI) (2023). *SAP2000 version 24.2.0.* California.

CSA (2019). *Engineering design in wood. CSA O86:19*. Canadian Standards Association, Toronto.

Das S., Tesfamariam S. (2022). Multiobjective design optimization of multi-outrigger tall-timber building: Using SMA-based damper and Lagrangian model, *Journal of Building Engineering*, 51: 104358.

Dires S., Tannert T. (2022). Performance of coupled CLT shear walls with internal perforated steel plates as vertical joints and hold-downs, *Construction and Building Materials*, 346: 128389.

Fang C., Wang W., Shen D. (2021). Development and Experimental Study of Disc Spring–Based Self-Centering Devices for Seismic Resilience, *Journal of Structural Engineering*, 147(7): 04021094.

Fernandez A., Komp J., Peronto J. (2020). Ascent - Challenges and Advances of Tall Mass Timber Construction. *International Journal of High-Rise Buildings*, 9(3), 235-244.

Feujofack K.B.V., Loss C. (2023). Finite-Element Modelling of a Novel High-Performance Shear Connector for Mass Timber Structural Assemblies, *Proceedings of the Canadian Society of Civil Engineering Annual Conference 2022 (CSCE2022)*, Lecture Notes in Civil Engineering, vol 348, 959-974.

FPInnovations (2019). *Canadian CLT Handbook*. https://web.fpinnovations.ca/wp-content/uploads/clt-handbook-complete-version-en-low.pdf. Accessed 10 October 2023.

Ganey R., Berman J., Akbas T., Loftus S., Dolan J.D., Sause R., Ricles J., Pei S., Lindt J.v.d., Blomgren H. (2017). Experimental Investigation of Self-Centering Cross-Laminated Timber Walls, *Journal of Structural Engineering*, 143(10): 04017135.

Halchuk S., Adams J., Kolaj M., Allen T., (2019). Deaggregation of NBCC 2015 Seismic Hazard for Selected Canadian Cities, *Proceedings of the 12th Canadian Conference on Earthquake Engineering*, Quebec, Canada.

Ibarra L.F., Krawinkler H. (2005). Global collapse of frame structures under seismic excitations, *Technical Report 152, The John A. Blume Earthquake Engineering Research Center, Department of Civil Engineering, Stanford University*, Stanford, CA.

Iqbal A., Pampanin S., Palermo A., Buchanan A.H. (2015). Performance and Design of LVL Walls Coupled with UFP Dissipaters, *Journal of Earthquake Engineering*, 19:3, 383-409.

Jilla C.D., Miller D.W. (2001). Assessing the performance of a heuristic simulated annealing algorithm for the design of distributed satellite systems, *Acta Astronautica*, 48(5): 529-543.

Karacabeyli E., Lum C. (2022). *Technical Guide for the Design and Construction of Tall Wood Buildings in Canada*, Vancouver: FPInnovations.

Mam K., Douthe C., Roy R.L., Consigny F. (2020). Shape optimization of braced frames for tall timber buildings: Influence of semi-rigid connections on design and optimization process, *Engineering Structures*, 216: 110692.

McKenna F., Scott M.H., Fenves G.L. (2010). Nonlinear finite-element analysis software architecture using object composition, *Journal of Computing in Civil Engineering*, 24(1):95-107.

Moerman B., Li M., Smith T., Lim H. (2022). Design and cyclic testing of bolted end plate connections between steel link beams and cross-laminated timber for coupled shear walls, *Construction and Building Materials*, 353: 129060.

naturally:wood (2016). Tallwood House Storyboards, https://www.naturallywood.com/wp-content/uploads/brock-commons-storyboards_factsheet_naturallywood.pdf, Accessed 25 May 2023.

NHERI Tall Wood (2023). http://nheritallwood.mines.edu/. Accessed 27 October 2023.

NRC (2020). *National Building Code of Canada (NBC) 2020.* National Research Council of Canada, Ottawa.

Ohsaki M. (2010). *Optimization of Finite Dimensional Structures*, Florida: CRC Press.

Oregon State University & Portland State University (OSU/PSU) (2017). Framework: An urban + rural ecology. Deliverable 18: Structural testing. https://www.thinkwood.com/wp-content/uploads/2018/10/18-Framework-Structural-Testing.pdf, Accessed 10 October 2023.

Poh'sie G.H., Chisari C., Rinaldin G., Amadio C., Fragiacomo M. (2016). Optimal design of tuned mass dampers for a multi-storey cross laminated timber building against seismic loads, Earthquake Engineering and Structural Dynamics, 45: 1977-1995.

Safarik D., Elbrecht J., Miranda W. (2022). State of tall timber 2022, https://www.ctbuh.org/resources/papers/4530-Journal2022_IssueI_StateofTallTimber/TBIN.pdf, 2022, Accessed 10 October 2023.

Shulman S., Loss C. (2023a). High-performance grout-reinforced shear connectors for hybrid steel-cross-laminated timber building systems: Experimental study. *Journal of Building Engineering*, 67, 106014.

Shulman S., Loss C. (2023b). Performance of a Grout-Reinforced Hybrid Steel-Timber Shear Connection for Mass Timber Buildings, *Proceedings of the Canadian Society of Civil Engineering Annual Conference 2021 (CSCE2021)*, Lecture Notes in Civil Engineering, vol 241, 341-352.

Teweldebrhan B.T., Tesfamariam S. (2022). Performance-based design of tall-coupled cross-laminated timber wall building, *Earthquake Engineering & Structural Dynamics*, 51(7): 1677-1696.

Yang T.Y., Lepine-Lacroix S., Ramos Guerrero J.A., McFadden J.B.W., Al-Janabi M.A.Q. (2022). Seismic performance evaluation of innovative balloon type CLT rocking shear walls, *Resilient Cities and Structures*, 1(1): 44-52.